How to Swoop and Grasp Like a Bird With a Passive Claw for a High-Speed Grasping

William Stewart, Enrico Ajanic, Matthias Müller, and Dario Floreano, *Senior Member, IEEE*

***Abstract*—There is a growing interest in unmanned aerial vehicles (UAVs) grasping, perching, and interacting with their surroundings by means of claws, arms, hooks, and other appendages. While multirotor vehicles can slowly lower onto a target object and grasp it, winged UAVs require a minimum speed to remain airborne and cannot hover. In this article, we describe a novel avian-inspired grasping mechanism that allows winged UAVs to grasp an object while flying over it. We have developed a high-speed, passively triggered claw that can close in under half a second. We characterize the loads encountered by the vehicle during the grasp event and find that grasping an object of about 30 g produces a maximum load of less than 12 N. Numerical experiments indicate that these loads cause a change in pitch of less than 1 ° and a decrease in speed of about 0.3 m/s for a fixed-wing vehicle of about 1 kg, and are thus negligible. We demonstrate outdoor in-flight grasping at 8 m/s, the fastest recorded grasping by a flying robot to date to best of our knowledge.**

***Index Terms*—Grasping, mechanical systems, unmanned Aerial Vehicles.**

Fig. 1. (Top) UAV with grasped object in the claw and (bottom) eagle having just grasped a fish. Photo of the bird adapted from [7].

I. Introduction

THERE are some spectacular videos of raptors rapidly swooping out of the sky to grasp prey midflight, both on land and from the water [1], [2]. By contrast, in the field of aerial robotics, a very different strategy, which was designed for the ubiquitous rotary-wing platforms, is used to pick up objects. Usually, unmanned aerial vehicles (UAVs) approach their target, come to a stop, lower themselves to the target, and grasp the object of interest [3]–[5]. This strategy, however, is not suitable for more efficient winged UAVs, which are generally unable to perform the hovering maneuver due to minimum speed requirements. To the best of our knowledge, there are no examples of fixed-wing UAVs capable of grasping an object. It is theoretically possible for a fixed-wing UAV to perform the same maneuver as a rotary-wing UAV, however, this requires vertical takeoff and landing (VTOL) capabilities. Fixed-wing UAVs have a longer range and endurance than rotary-wing UAVs, but including the added mass and complexity of VTOL mechanisms reduces that advantage [6]. Therefore, to be able to grasp and carry an object a long distance or for a long time requires a fundamental reconsideration of the grasping strategy. In this article, we study the mechanics of implementing object grasping on fixed-wing UAVs through the use of a swooping strategy inspired by birds of prey (see Fig. 1).

Similar to the talons of birds of prey [8] and motivated by recent research indicating that birds curve their claws to reliably grasp a branch when perching [9], we propose a claw design that is composed of three curved talons. The design of a claw for a swooping UAV must satisfy at least three design criteria: fast response time, reliable grasping, and the ability to hold the object during flight, all while being low weight and low power. The claw developed here (see Fig. 3) incorporates a spring-driven mechanism to rapidly and passively close around the object. The inner surfaces of the talons are padded by velcro in order to increase grasping and holding reliability. The claw is made of lightweight composite materials, such as fiberglass and carbon

Manuscript received June 11, 2021; revised September 27, 2021; accepted November 17, 2021. Recommended by Technical Editor S. Foong and Senior Editor H. Qiao. This work was supported in part by Intel Network on Intelligent Systems, in part by the Swiss National Science Foundation through the National Centre of Competence in Research (NCCR), and in part by the European Union's Horizon 2020 research and innovation programme under Grant 871479 AERIAL-CORE. *(Corresponding author: William Stewart.)*

William Stewart, Enrico Ajanic, and Dario Floreano are with the Laboratory of Intelligent Systems, Ecole Polytechnique Federale de Lausanne, CH1015 Lausanne, Switzerland (e-mail: william.stewart@epfl.ch; enrico.ajanic@epfl.ch; dario.floreano@epfl.ch).

Matthias Müller is with the Intelligent Systems Laboratory, Intel, 85579 Neubiberg, Germany (e-mail: matthias.mueller@intel.com).

This article has supplementary material provided by the authors and color versions of one or more figures available at https://doi.org/10.1109/TMECH.2022.3143095.

Digital Object Identifier 10.1109/TMECH.2022.3143095

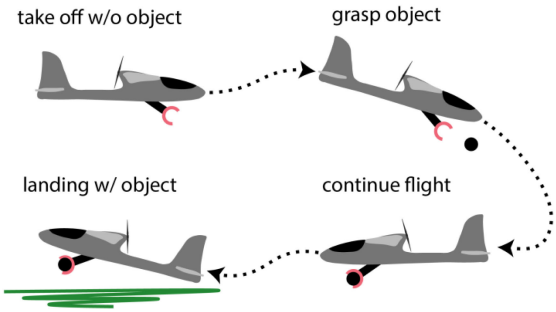

Fig. 2. Diagram showing a potential mission for the grasping mechanism developed here.

fiber, with minimal use of 3-D-printed parts. The claw was developed with winged UAVs in mind, however, the design is platform agnostic, and can be implemented in a quadrotor vehicle without any modifications (see the supplementary video). In total, the claw has a mass of only 35 g and has a closing time of between 0.08 and 0.35 s. For comparison, the actively triggered claw in [10] (the only UAV claw that reports a closing time) takes approximately 0.1 s to close, but weighs 551 g, similarly to other UAV claws [5], [10], [11].

In this article, we use an experimental test bench to recreate flight conditions at the moment of impact, and measure the magnitude and time span of loads exerted on the claw. Next, we use the measured loads to simulate their effect on aircraft dynamics. Finally, we conduct flight tests with the claw integrated in a winged aircraft and perform a swooping maneuver at high speeds ($\sim$8 m/s) to grasp a 34-g object.

The main contributions of this article are the following:

1) A novel passive claw concept for implementing the raptor inspired swooping strategy for fixed-wing UAVs.
2) Characterization of forces during a grasp with the swooping strategy.
3) Experimental validation of our claw prototype and swooping strategy in a realistic environment.

II. Related Work

The use of the swooping strategy for multirotor UAVs has been studied by Spica *et al.* [12]. The aim of their work was to grasp a moving object, which required them to rethink the stop, grasp, and restart approach. Though insightful, this project was only done in simulation. Another study was done by Thomas *et al.*, this time using a physical quadcopter to swoop and grasp an object [13]. However, their focus was on visual identification and control, instead of the mechanical aspects of grasping. Another study, by Tanaka *et al.*, investigated the economics of commercial UAVs performing the swooping strategy, which they refer to as nonstop parcel loading [14]. Their solution consisted of a robotic hand holding a bag up that could be grasped by a hook attached to a passing quadcopter. The drawback is that a ground-station necessitates preplanned and prebuilt infrastructure. Both Thomas *et al.* [13] and Tanaka *et al.* [14] implemented their solutions on indoor quadcopter flights. Due to space constraints, flying indoors typically limits the maximum attainable flight speed. At the same time, quadcopters can fly very slowly or even hover in place. As a result, the experiments were conducted at low speeds (1–3 m/s). Due to this, the forces these quadcopters encountered were low, and thus, did not require a study of the effects on aircraft dynamics.

For an aircraft with a mass of about 1 kg and high aspect ratio wings, a reasonable range of stall speed would be about 8–10 m/s (such as the aircraft in [15]). This is more than twice the speed range of the quadcopter systems developed by Thomas *et al.* [13] and Tanaka *et al.* [14]. As a result of this higher speed, the forces experienced by winged vehicles are higher than those experienced by those quadcopters. These higher forces have the potential to destabilize the aircraft, and possibly cause a crash. Therefore, for winged UAVs, it is important to characterize the impact loads generated by grasping and understand their effects on aircraft dynamics.

Impact loads have been studied and simulated before, however, the mechanics are complicated and rely on a litany of parameters, which depend on mechanical and material properties that must be validated for each system [16]. This makes the practical use of these models difficult. As an alternative, we use here an experimental method to characterize impact loads that is not reliant on the fine tuning of lots of design-specific parameters. In particular, we start with a bench-top test to first characterize the time required to close the claw, then move to a high-speed test setup to measure the impact force, and finally, use the measured forces simulate the effects of grasping on an UAV.

The literature abounds with examples of UAVs with integrated appendages that could be used to grasp objects [17], [18]. There are actively actuated appendages, such as arms installed on multirotor vehicles. These arms usually have many degrees of freedom (DoF), many actuators, and can exert a lot of force [5], [11], [19]. However, this makes them complex, heavy, and energy inefficient. To simplify and shrink these systems, other researchers have reduced weight by mounting claws directly to the bottom of the vehicle; they used them to turn valves [20] and manipulate objects [21]. The vehicle needs to be stationary during manipulation, a tradeoff that prevents its use on a fixed-wing platform. More exotic appendage designs include suction cups [22] or needles [23] to attach to doors and walls. Unfortunately, suction cups need to be precisely aligned, which can be challenging while moving fast, and picking an object up with needles could damage the object.

To avoid the weight, complexity, and power consumption of actuators, a number of designs have incorporated passive components such as prestressed elements [24]. However, prestressed elements have a limited range of motion due to their high-stiffness components. Some graspers are built into the vehicle structure, such as microspines used to open doors [25] or perch on vertical surfaces [26]. While completely passive, microspines are difficult to manufacture and must be kept clean to function properly. Other perching mechanisms developed for fixed-wing UAVs could potentially be used to grasp, such as needles [23] or a sticky pad [27]. However, the needles could

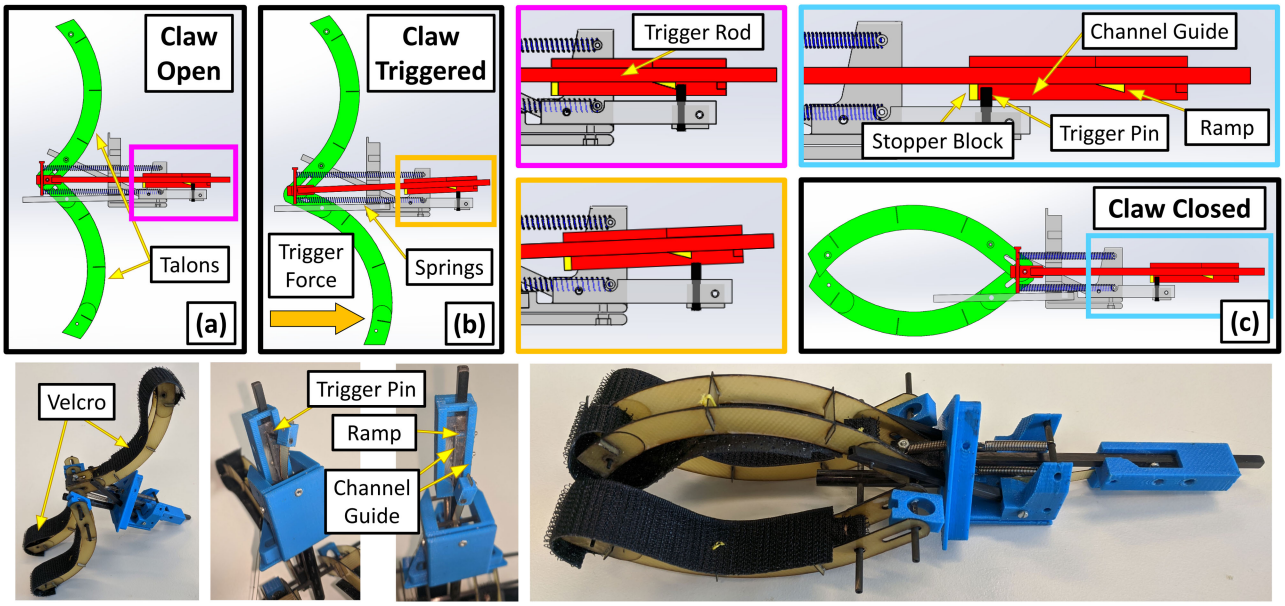

Fig. 3. (Top) Diagrams of the claw operation and (bottom) photos of the real prototype. (Top) In the CAD drawings of the claw, the rigid structure is shown in gray, the talons (without velcro) are in green, two sets of springs are in blue, the trigger rod is in red, and the ramp, which holds the claw open against the spring forces is in yellow. (a) Claw in the open position, prior to impact. The purple inset shows the trigger pin (in black) being pulled (by the blue stretched springs) against the back of the ramp (in yellow). (b) Claw acted on by the triggering force when grasping the object. The orange inset shows that the trigger force has dislodged the trigger rod (in red) from the trigger pin. At this point, the stretched springs push the trigger rod backwards resulting in the state of the claw shown in (c). (Bottom) Photos depict (from left to right) the complete claw opened, the back of the claw opened, the back of the claw closed, and the complete claw closed.

damage the object, and the sticky pad needs enough surface area and impact time to properly stick to the object.

III. Claw Operating Principle

When the UAV is initially launched, the claw is open and empty (see Fig. 2). The UAV navigates to the object and conducts a swooping maneuver to grasp the object without stopping. The UAV then continues flight, either to return to the starting point or deliver the object to another location. Upon arrival at the delivery point, the UAV lands, allowing users to unload it. Many realistic applications follow such a mission pattern, such as sending the UAV to fetch a tool, or using the UAV to deliver scientific or medical samples.

The operating principle of the claw is simple. The three fiberglass talons are pulled closed by two sets of two springs in series. The claw is held open by a trigger pin that is hooked on the end of a ramp, which in turn is attached to a trigger rod [see Fig. 3(a)]. The trigger rod is the interface between the talons and the trigger pin. The closing of the claw is triggered when one of the two lower talons contacts an object. This creates a moment that pulls on the trigger rod [see Fig. 3(b)], which dislodges the ramp from the trigger pin, releasing the springs that snap the talons closed [see Fig. 3(c)]. As the claw closes, the trigger rod slides backwards, away from the talons, until the stopper block contacts the trigger pin and the claw is completely closed [see Fig. 3(c)]. Channel guides keep the trigger rod aligned with the trigger pin during this motion. Pushing the trigger rod forward again will simultaneously open the talons and push the trigger pin up the ramp, where it will get hooked again. Thus, the trigger mechanism can be reset.

The triggering of the claw is dependent on the friction force between the trigger pin and the ramp. To trigger the closing of the claw, the impact force (F_{imp}) of the claw must be high enough to overcome the friction between the trigger pin and ramp (see Fig. 4). The friction force can be written as

$$F_{\text{fric}} = \mu F_R = \mu 2 F_s = \mu 2 k s \tag{1}$$

where μ is the coefficient of friction, F_R is the reaction force from the springs, F_s is the force from one set of 2 springs in series, ks is the spring constant multiplied by the stretch of the springs, and the factor of 2 results from the two sets of springs.

The impact force, which must overcome the friction force, happens at a distance d_1 from the pin on the claw talon. This causes force F to pull on the trigger rod, creating a moment about the slot. This moment due to the impact force will balance with the friction force at the instant of triggering. The equation for this moment balance based on the free body diagram in Fig. 4 is

$$F d_3 = F_{\text{fric}} d_4 \tag{2}$$

where the force F is a function of the distance between the impact force and the pin on the talon.

$$F = F_{\text{imp}} \frac{d_1}{d_2}. \tag{3}$$

Combining (1) and (3) into (2) gives the minimum force required to trigger the claw based on claw design parameters.

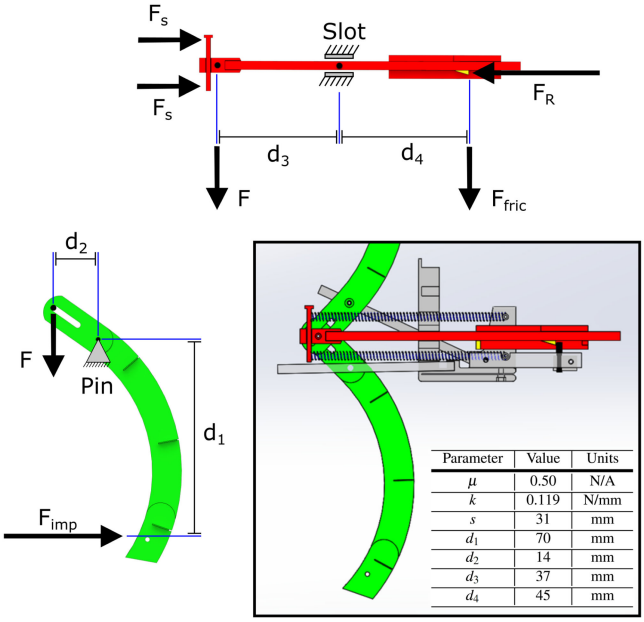

Fig. 4. Free body diagram of the claw illustrating relevant forces and distances. In green are the talons, in red is the trigger rod, and in gray is the fixed structure.

These parameters are k the spring constant, μ the friction between the trigger pin and ramp (which is a material and geometry choice), and distances (which are a claw geometry choice).

$$F_{\text{imp}} = \mu(2)ks\frac{d_2 d_4}{d_1 d_3}. \tag{4}$$

The minimum triggering force, F_{imp}, for the claw built for this project is 0.89 N. This force should be large enough that the triggering does not happen inadvertently, but small enough that the claw will trigger on impact. When characterizing the impact loads during grasping (see Section V), we found that this force was low enough to enable proper triggering and we found during flight testing (see Section VII) that this force was high enough to prevent premature triggering.

IV. Closing Speed Characterization

In this section, we investigate how factors like the spring stiffness, trigger location, object weight, and object diameter affect the closing speed. The claw was fixed to a custom test bench facing up and cylindrical test objects were dropped onto the claw [see Fig. 5(a)]. Each object was dropped by hand from a distance of 30 cm, causing the claw to trigger and close. The object diameters tested were 30, 50, 65, 85, and 100 mm, while the weights were 20, 30, 40, and 50 g. The objects had strips of velcro attached to them to connect with the strips of velcro on the talons. The objects were chosen to be representative of a small tool or material sample that may be transported by a small-scale UAV. The total time of the claw closing was found by counting the number of high-speed video frames between impact [see Fig. 5(b)] and the claw being completely closed [see Fig. 5(c)]. Video was recorded with a Chronos high-speed camera at 100 ft/s, and each experiment was conducted ten times.

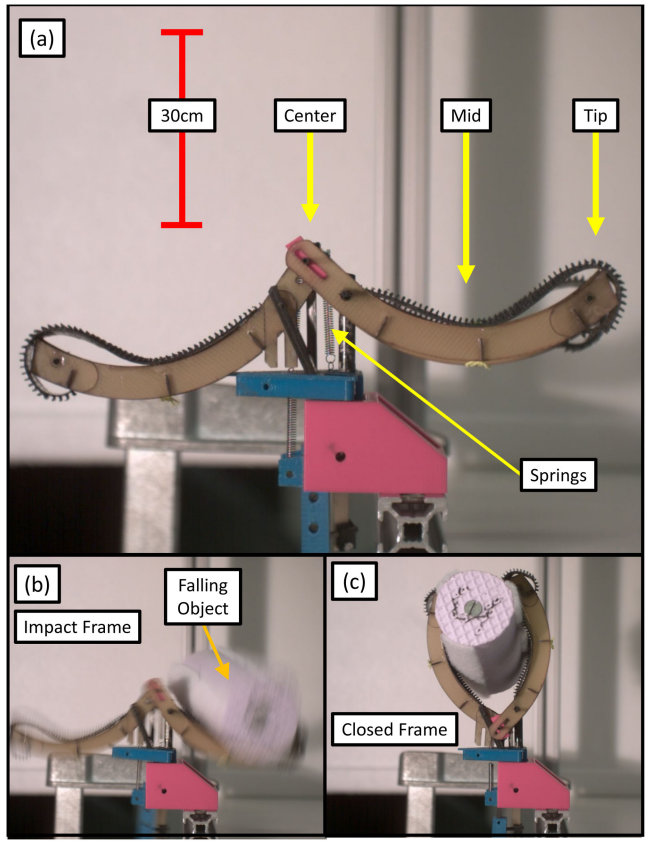

Fig. 5. Closing speed test setup. (a) Open claw mounted to a test bench. Objects are dropped 30 cm onto the claw at different locations (indicated by yellow arrows). (b) Example impact frame from the high-speed video. (c) Example frame when the claw is closed.

The first factor investigated is the stiffness of the springs driving the closing motion. We investigated this by swapping in springs of five different stiffnesses (0.041, 0.119, 0.318, 0.424, and 0.637 N/mm) into the claw and repeating the experiments. The stiffer the springs, the more force they will exert to close the claw, causing the talons to close faster [see Fig. 6(a)]. However, this reduction of closing time comes with diminishing returns. That is, the decrease in closing time achieved for a given increase in stiffness is lower at higher spring stiffness. For instance, increasing the spring stiffness by 290% from 0.041 to 0.119 N/mm reduces the closing time by about 40%, or 0.08 s. However, increasing the spring stiffness further from 0.119 to 0.637 N/mm (535%) decreases closing time by only about 0.04 s (33%).

The second investigated factor is where the object triggers the closure. For this experiment, three locations were chosen, the center of the claw, the middle of the talon, and the tip of the talon [see Fig. 6(b)]. As the trigger location moves out along the talon from the center of the claw, the closing time increases. This is because if the object triggers the closing at the tips of the talons, then the inertia of the object will oppose the closing force of the talons, thereby slowing the closing speed.

The third factor tested was object weight. This was tested by dropping the objects of differing weight on the claw. The heavier

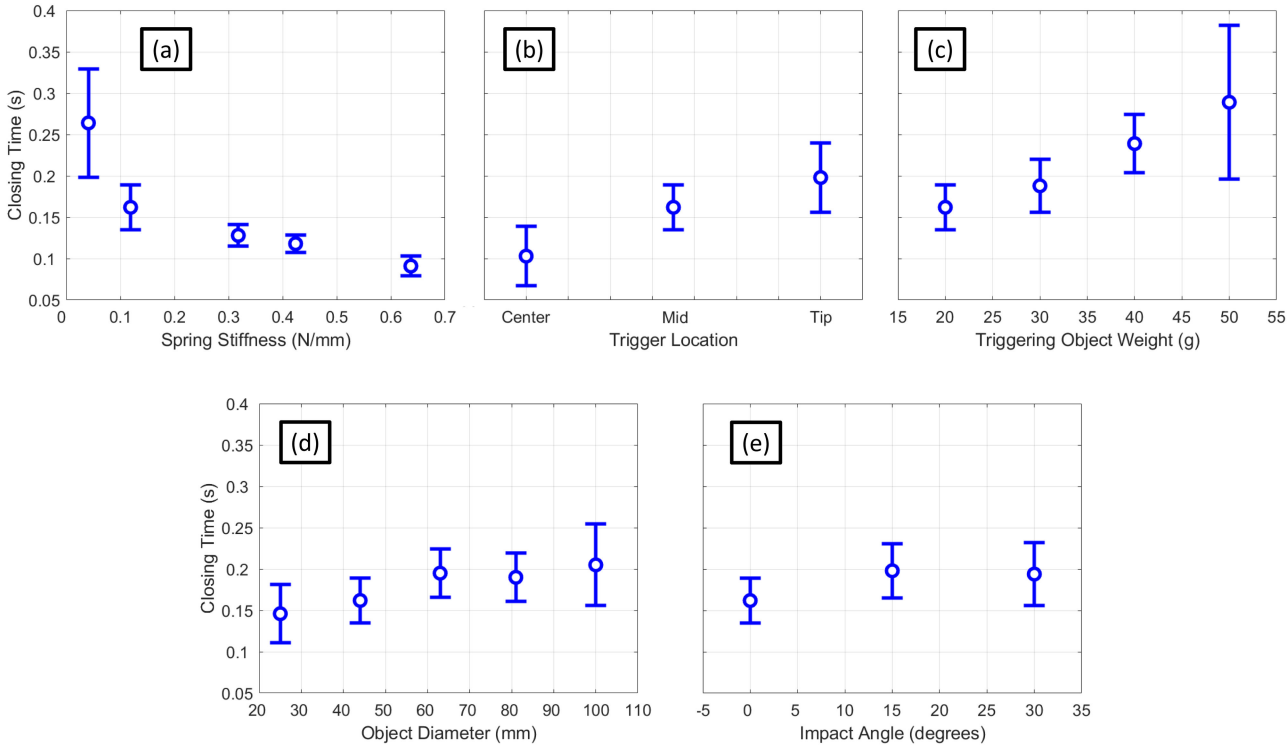

Fig. 6. Closing speeds at a variety of conditions. The blue circles indicate the average of ten runs and the blue bars indicate the standard deviation. (a) Variation with spring stiffness (20-g/50-mm object at the middle of the talon). (b) Variation with trigger location (20-g/50-mm object with 0.119-N/mm spring stiffness). (c) Variation with object mass (30-mm object at the middle of the talon with 0.119-N/mm spring stiffness). (d) Variation with object diameter (20-g object at the middle of the talon with 0.119-N/mm spring stiffness). (e) Variation with impact angle (20-g/50-mm object at the middle of the talon with 0.119-N/mm spring stiffness).

the object, the more inertia it has, and the more the claw closing is slowed down [see Fig. 6(c)].

The fourth factor was object diameter [see Fig. 6(d)]. The increasing object diameter gives the object an increasing volume. This factor had little effect on the closing time of the claw.

The final factor investigated was impact angle [see Fig. 6(e)]. Sometimes the UAV will not hit the object perfectly straight on. This can happen when the UAV has some roll or yaw angle. In these cases, the object will hit one talon before the other and this could affect the closing performance. To test this, we mounted the claw at an angle and dropped the objects straight down on it. Three angles were tested, 0°, 15°, and 30°. The results showed that the angle at which the vehicle grasps the object does not have a large effect on closing time.

Over the course of all of these experiments, we found that the closing time can range between about 0.08 and 0.35 s (see Fig. 6).

V. Impact Force Characterization

The characterization of the forces expected at grasping is required to understand the effects on the aircraft flight. To characterize the impact forces, the claw was mounted to an ATI Nano25 6DoF load cell and attached to the end of a boom [see Fig. 7(a)], which in turn was mounted through bearings to a robotic arm [see Fig. 7(b)]. During the test, the robot rotated an actuated structure, which pushed the boom and claw around toward a waiting test object. The robot stopped rotating just before the impact, allowing the boom to swing freely into the object. Because the boom was free to swing, the measured forces better match the forces experienced by an aircraft than if the robot arm forced the boom through the grasping event. This is because both the boom and the aircraft are free to move during and after the impact. The z-axis of the load cell was aligned with the boom (normal to the arc of the swing) and the x-axis was tangential to the motion. The object was positioned at the lowest point in the motion arc, which corresponds to a vertical alignment of the load cell z-axis. Tests were done at 6.0, 8.4, and 9.4 m/s as measured by an Optitrack Motion Capture System. These speeds correspond to the approximate stall speed of a moderately sized fixed-wing UAV such as the senseFly eBee (6–7 m/s) or Hobby King Bixler 3 (8–10 m/s). For these experiments and the following ones, the claw was equipped with springs of stiffness 0.119 N/mm and the object used has a mass of 34 g. We also performed control experiments without the object for each speed.

From the z-axis load cell data of individual runs, we can see a sharp increase in force at the beginning up to a maximum point (see Fig. 8). Then, a slower decrease in force until it reaches a minimum. Regardless of the speed of the impact, the maximum forces measured here vary only by a few Newtons. Throughout all the experiments, the measured loads are below 12 N total. The entire three-phase grasping event takes place between 0.25 and 0.32 s, decreasing a small amount with increasing flight

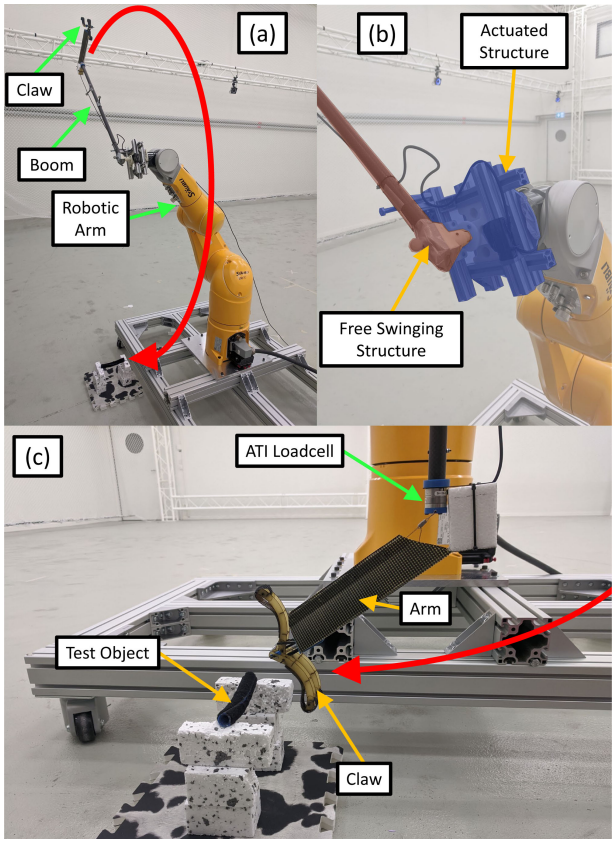

Fig. 7. Impact force test setup. (a) Robotic arm and boom. The red arrow indicates the motion of the boom and claw. (b) Close-up photo of the robotic arm. Highlighted in blue is the actuated structure, which is rotated by the robot arm. In red is the boom, which is mounted on bearings allowing it to swing freely. (c) Close-up photo of the test object being grasped and the claw position just before grasping.

TABLE I
COMPARISONS OF GRASPING AND CLOSING TIME SPANS

	6m/s	8.4m/s	9.4m/s
Impact phase	0.05s	0.05s	0.04s
Adjustment phase	0.12s	0.10s	0.11s
Settling phase	0.15s	0.12s	0.10s
Total grasping event	0.32s	0.27s	0.25s

speed (see Table I). These grasping event time spans correspond closely with the speed at which the claw can close, which was found to be between 0.08 and 0.35 s in Section IV.

VI. Impact Load Effects on Aircraft Dynamics

The ultimate aim of characterizing the forces at impact is to understand how they affect the flight of the aircraft during and immediately after the grasp. To this end, a dynamic simulation of an aircraft was created using the Simulink 6DOF EoM block from the Aerospace Blockset . The simulation does not include a feedback controller. The simulated aircraft was a Hobby King Bixler 3 (see Fig. 1) with additional mass for an appendage consisting of a short arm holding the claw. Moments of inertia were estimated using a series of point masses and a physical version of the aircraft.

The aircraft was first simulated flying in straight and level trimmed flight for 20 s. Then, the forces previously measured were applied to the aircraft at the center of gravity (CG). The simulation used the forces measured in all three directions of the load cell. A linear interpolation was used between the preimpact mass properties and postimpact mass properties.

The grasping creates a spike in linear velocity and attitude across the three dimensions of roll, pitch, and yaw [see Fig. 9(a) and (b)]. Following the grasp, an oscillation is induced. The biggest effects of the impact are on forward speed [black line in Fig. 9(a)] and pitch angle [black line in Fig. 9(b)]. When applied at the CG, the impact loads produce a pitch-up moment. In low speed, high angle of attack flight, such as when trying to grasp an object, this pitch-up moment could stall the aircraft and cause a crash. This can be countered by changing the moment arm of the impact loads by moving the mount point along the fuselage of the aircraft.

To study the effects of moving the mount point of the appendage forward and backward, the simulation was repeated by changing the application location of the loads. These variations [see Fig. 9(c)] result in postimpact oscillations too. However, shifting the loads forward exacerbates the initial jerk in the pitch angle, while shifting the loads backwards reduces the peak pitch spike. This implies that placing the appendage at the CG will give the smoothest pickup. Moving the appendage back a little ($\sim$5 cm), however, could reduce the maximum magnitude in pitching motion. Of all the mounting locations studied here, none of the pitching motions were enough to stall the aircraft. In fact, the overall change in pitch for an aircraft such as the Bixler 3, was quite low and amounted to less than 0.2°. All together, these results suggest that a small-scale UAV, such as the Bixler 3 equipped with the claw, could grasp objects with a weight on the order of tens of grams in-flight without risking a crash.

VII. Flight Testing

As a proof-of-concept, we performed a flight in a realistic outdoor environment with a real aircraft, the popular fixed-wing platform Bixler 3 [see Fig. 10(a)]. A short arm with a built-in hinge connected the claw to the bottom of the fuselage 8-cm forward of the CG. The aircraft was equipped with a Pixhawk 4 for data recording, a GPS sensor, and a Pitot tube for airspeed measurements. In total, the aircraft had a mass of 1.061 kg before grasping the object. Throughout the flight, the aircraft was manually flown toward a 34-g tubular object, which rested atop a forked support. The object was approximately 1 m above the ground.

Due to natural variation in human piloting and nonuniform wind, multiple flights with grasping could not be compared with one another, so only a single flight was conducted. Over the course of the final approach [Time $= -8$ to 0 s in Fig. 10(c)], the pitch varied about half a degree. At impact, the aircraft began a pitch down motion. However, due to the high pitch variability on the final approach, it is impossible to correlate this motion with the grasp. Before impact, the velocity of the aircraft was approximately 8 m/s with variations of up to 1 m/s. However,

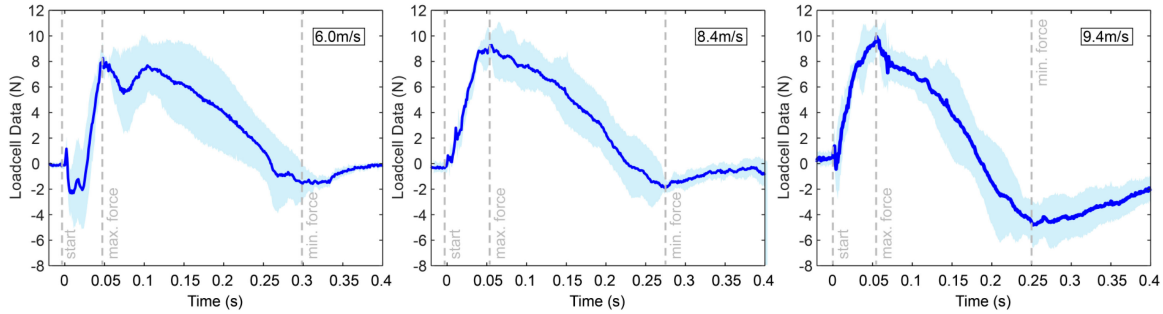

Fig. 8. Plots showing the mean impact forces (blue line) and the standard deviation (blue shaded area) from three trials for three different impact velocities of 6.0, 8.4, and 9.4 m/s. To ensure that only the effects of the grasp are captured, the data here are the difference between the load cell data measured during an experiment when the object was grasped and a control experiment when no object was grasped.

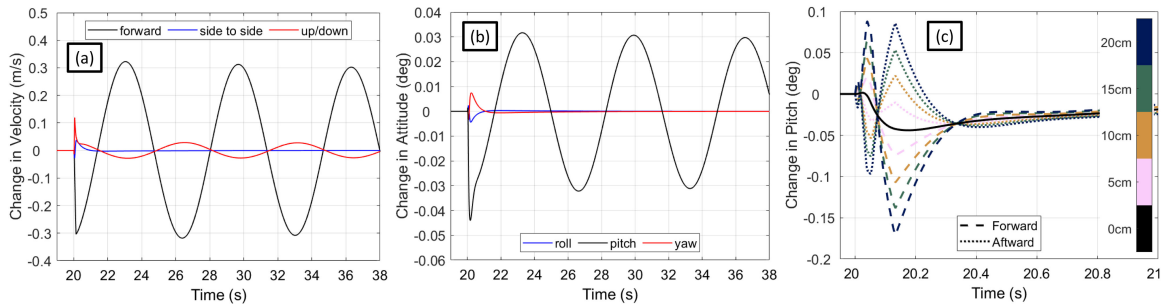

Fig. 9. Results of the simulated pickup using the data from the force characterization experiment at 8.4-m/s impact speed. Impact occurs 20 s after the start of the simulation. (a) and (b) Plots showing induced oscillations from the grasping event when the force is applied at the CG. (c) Zoomed in plot showing the effects of moving the appendage (mounting point of the claw) forward or backward along the fuselage.

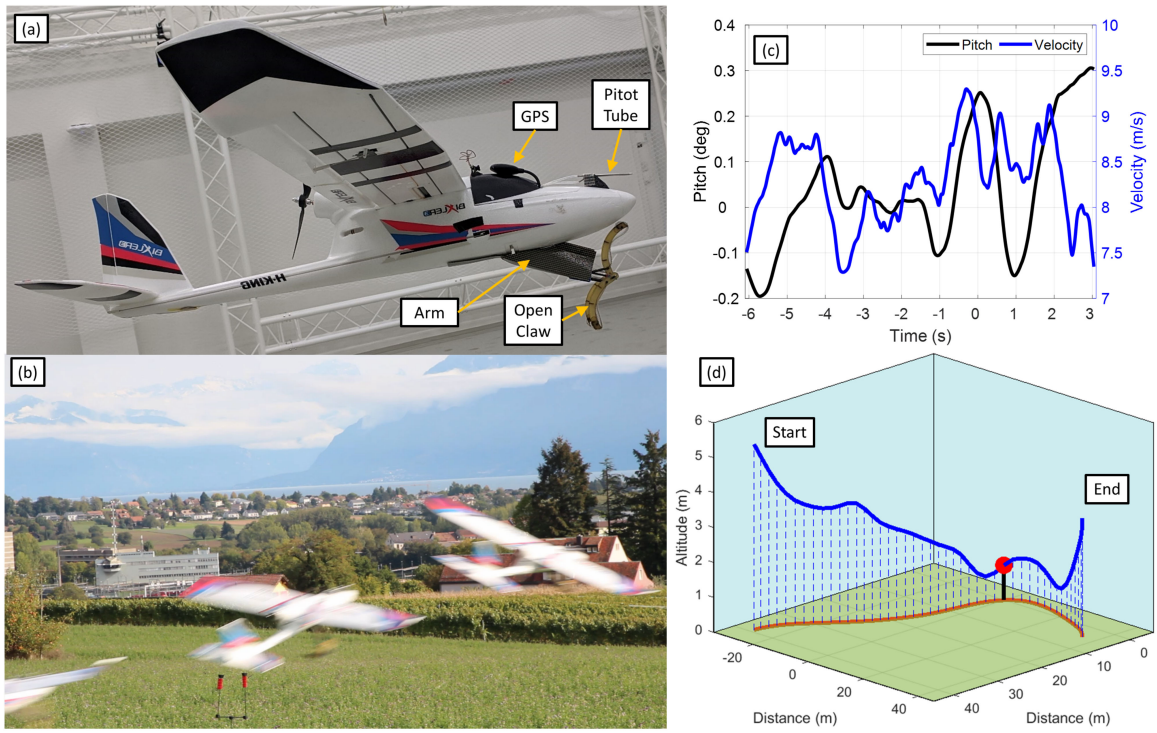

Fig. 10. Flight test aircraft and data. (a) Photo of the modified Bixler 3 with an arm, claw, and avionics. Inside the fuselage is a Pixhawk 4 autopilot used to record attitude, altitude, position, and velocity. (b) Composite image of the aircraft performing the grasp. (c) Vehicle state over the time period of approach and grasp. Time on the *x*-axis is zeroed at the moment of grasp. In black is the pitch angle and in blue the velocity. (d) Three-dimensional view of the trajectory in blue. The fork holding the object is represented with a black line and the object itself is indicated with a red dot.

as with the pitch angle, there was no significant change after the grasp.

Although only a single flight was conducted, the findings are in line with the effects seen in the simulation. For example, the simulation predicts pitch oscillations will occur with magnitudes of hundredths of a degree. It also predicts that the aircraft will slow by tenths of an m/s. The changes in aircraft velocity observed in flight tests are dominated by imperfections of manual teleoperation and wind disturbances. Because the perturbations resulting from the grasp were small, the UAV is capable of flying away with the object firmly secured in the claws.

A video of the outdoor flight can be found in the supplementary video. To demonstrate the generality of the claw and concept, a short flight was also conducted with the claw on a quadcopter. This flight was conducted at low speeds (1 m/s) and was also manually piloted. The quadcopter flight is also included in the supplementary video.

VIII. Conclusion

In this article, we studied the mechanics of an UAV swooping and grasping like a bird. We have proposed a new claw design that is lightweight, passive, and rapidly closing. With this claw, we characterized the force in terms of magnitude and time, finding that the maximum magnitude and time frame of the impact event is resilient to changes in vehicle speed (magnitude less than 12 N and time frame less than half a second). We see that there is an asymmetric loading, where the load increases rapidly to a maximum, then more slowly reduces down to a minimum. As a result of this, a simple impact model based on variations in momentum or work and energy that predicts an average force is unlikely to accurately capture the effect of grasping on a swooping aircraft.

These measurements give engineers a frame of reference for the development of future grasping mechanisms. Our experimental methodology lays out a systematic approach to developing these mechanisms from simple, initial tests to vehicle implementation that does not require precise material parameter validation. The claw design developed in this work may serve as the basis for passive object grasping for all types of aerial robots, including fixed-wing, rotary-wing, and flapping wing vehicles (see the supplementary video file for grasping flights with both a fixed-wing drone and a quadcopter). The methods and results described here could be used to optimize the gripper for specific platforms and uses with respect to mass, stiffness, and dimensions, to name a few aspects. While the swoop and grasp strategy described here requires precise control, future developments in visual servoing and vision-based navigation may lead to entirely autonomous drones with bird-like grasping abilities.

Acknowledgment

The authors are grateful for the engineering help provided by V. Wüest and O. Gudozhnik. They also wish to thank Pr. Kornatowski for his help and excellent piloting skills.

References

[1] "Red Kites in Slow Motion—The Slow Mo Guys," Accessed: Sep. 2021, [Online]. Available: https://youtu.be/AYOx-iCMZhk

[2] "BBC One - Nature's Great Events, The Great Salmon Run," Accessed: Sep. 2021, [Online]. Available: https://www.bbc.co.uk/programmes/b00hq341

[3] Y. Mulgaonkar *et al.*, "The flying monkey: A mesoscale robot that can run, fly, and grasp," in *Proc. IEEE Int. Conf. Robot. Automat.*, May 2016, pp. 4672–4679.

[4] P. E. I. Pounds, D. R. Bersak, and A. M. Dollar, "Grasping from the air: Hovering capture and load stability," in *Proc. IEEE Int. Conf. Robot. Automat.*, May 2011, pp. 2491–2498.

[5] G. Heredia *et al.*, "Control of a multirotor outdoor aerial manipulator," in *Proc. IEEE/RSJ Int. Conf. Intell. Robots Syst.*, Sep. 2014, pp. 3417–3422.

[6] R. Chiappinelli and M. Nahon, "Modeling and control of a tailsitter UAV," in *Proc. Int. Conf. Unmanned Aircr. Syst.*, Jun. 2018, pp. 400–409.

[7] A. Hyde, "White-tailed eagle (Haliaeetus albicilla), swooping to take a fish from the water's surface,", Accessed: Sep. 2021. [Online]. Available: https://www.naturepl.com/stock-photo-white-tailed-eagle-haliaeetus-albicilla--swooping-to-take-a-fish-from-image01530847.html

[8] L. R. Tsang, L. A. B. Wilson, J. Ledogar, S. Wroe, M. Attard, and G. Sansalone, "Raptor talon shape and biomechanical performance are controlled by relative prey size but not by allometry," *Sci. Rep.*, vol. 9, no. 1, pp. 7076–7086, May 2019.

[9] W. R. Roderick, D. D. Chin, M. R. Cutkosky, and D. Lentink, "Birds land reliably on complex surfaces by adapting their foot-surface interactions upon contact," *eLife*, vol. 8, Aug. 2019, Art. no. e46415.

[10] A. McLaren, Z. Fitzgerald, G. Gao, and M. Liarokapis, "A passive closing, tendon driven, adaptive robot hand for ultra-fast, aerial grasping and perching," in *Proc. IEEE/RSJ Int. Conf. Intell. Robots Syst.*, Nov. 2019, pp. 5602–5607.

[11] S. Kim, S. Choi, and H. J. Kim, "Aerial manipulation using a quadrotor with a two DOF robotic arm," in *Proc. IEEE/RSJ Int. Conf. Intell. Robots Syst.*, Nov. 2013, pp. 4990–4995.

[12] R. Spica, A. Franchi, G. Oriolo, H. H. Bülthoff, and P. R. Giordano, "Aerial grasping of a moving target with a quadrotor UAV," in *Proc. IEEE/RSJ Int. Conf. Intell. Robots Syst.*, Oct. 2012, pp. 4985–4992.

[13] J. Thomas, G. Loianno, J. Polin, K. Sreenath, and V. Kumar, "Toward autonomous avian-inspired grasping for micro aerial vehicles," *Bioinspiration Biomimetics*, vol. 9, no. 2, May 2014, Art. no. 025010.

[14] S. Tanaka, T. Senoo, and M. Ishikawa, "High-speed UAV delivery system with non-stop parcel handover using high-speed visual control," in *Proc. IEEE Intell. Transp. Syst. Conf.*, Oct. 2019, pp. 4449–4455.

[15] A. Waldock, C. Greatwood, F. Salama, and T. Richardson, "Learning to perform a perched landing on the ground using deep reinforcement learning," *J. Intell. Robot. Syst.*, vol. 92, no. 3, pp. 685–704, Dec. 2018.

[16] P. Flores and H. M. Lankarani, *Contact Force Models for Multibody Dynamics* (Solid Mechanics and Its Applications). Berlin, Germany: Springer, 2016.

[17] F. Ruggiero, V. Lippiello, and A. Ollero, "Aerial manipulation: A literature review," *IEEE Robot. Automat. Lett.*, vol. 3, no. 3, pp. 1957–1964, Jul. 2018.

[18] H. B. Khamseh, F. Janabi-Sharifi, and A. Abdessameud, "Aerial manipulation literature survey," *Robot. Auton. Syst.*, vol. 107, pp. 221–235, Sep. 2018.

[19] S.-J. Kim, D.-Y. Lee, G.-P. Jung, and K.-J. Cho, "An origami-inspired, self-locking robotic arm that can be folded flat," *Sci. Robot.*, vol. 3, no. 16, Mar. 2018, Art. no. eaar2915.

[20] M. Orsag, C. Korpela, S. Bogdan, and P. Oh, "Valve turning using a dual-arm aerial manipulator," in *Proc. Int. Conf. Unmanned Aircr. Syst.*, May 2014, pp. 836–841.

[21] T. W. Danko, K. P. Chaney, and P. Y. Oh, "A parallel manipulator for mobile manipulating UAVs," in *Proc. IEEE Int. Conf. Technol. Practical Robot Appl.*, May 2015, pp. 1–6.

[22] H. Tsukagoshi, M. Watanabe, T. Hamada, D. Ashlih, and R. Iizuka, "Aerial manipulator with perching and door-opening capability," in *Proc. IEEE Int. Conf. Robot. Automat.*, May 2015, pp. 4663–4668.

[23] M. Kovac, J. M. Germann, C. Hürzeler, R. Siegwart, and D. Floreano, "A perching mechanism for micro aerial vehicles," *J. Micro-Nano Mechatronics*, vol. 5, no. 3-4, pp. 77–91, May 2010.

[24] D. Mellinger, Q. Lindsey, M. Shomin, and V. Kumar, "Design, modeling, estimation and control for aerial grasping and manipulation," in *Proc. IEEE/RSJ Int. Conf. Intell. Robots Syst.*, Sep. 2011, pp. 2668–2673.

[25] M. A. Estrada, S. Mintchev, D. L. Christensen, M. R. Cutkosky, and D. Floreano, "Forceful manipulation with micro air vehicles," *Sci. Robot.*, vol. 3, no. 23, Oct. 2018, Art. no. eaau6903.
[26] H. Jiang *et al.*, "Modeling the dynamics of perching with opposed-grip mechanisms," in *Proc. IEEE Int. Conf. Robot. Automat.*, May 2014, pp. 3102–3108.
[27] M. Anderson, "The sticky-pad plane and other innovative concepts for perching UAVs," in *Proc. 47th AIAA Aerosp. Sci. Meeting New Horiz. Forum Aerosp. Expo.*, 2009, pp. 40–50.

William Stewart received the M.S. and Ph.D. degrees in aerospace engineering from North Carolina (NC) State University, Raleigh, NC, USA, in 2014, and 2018, respectively.

From 2010 to 2014, he was a leader of the NC State University Aerial Robotics Team. From 2014 to 2016, he worked as a Research Assistant on the Eagle Ray project with the Smart Composites Laboratory. Since 2018, he has worked as a Postdoctoral Researcher with the Laboratory of Intelligent Systems, Swiss Federal Institute of Technology Lausanne, Lausanne, Switzerland. His research interests include aerodynamics, mechanics, and vehicle design.

Dr. Stewart was two time AUVSI student UAS competition champion (2010 and 2014).

Enrico Ajanic received the B.Eng. degree in mechanical engineering from Kempten University, Kempten, Germany, in 2015, and the M.Sc. degree in mechanical and aerospace engineering from the University of Nottingham, Nottingham, U.K., in 2017. He is currently working toward the Ph.D. degree with the Swiss Federal Institute of Technology Lausanne, Lausanne, Switzerland .

He has extensive experience in designing, manufacturing, and testing of fixed-wing and morphing drones. His research interests include the fields of aerodynamics, flight mechanics, behavioral biology of birds, and aerial robotics.

Matthias Müller received the B.Sc. degree in electrical engineering and math minor from Texas A&M University, College Station, TX, USA, in 2011, and the M.Sc. degree in electrical engineering, in 2016, and Ph.D. degree in sim-to-real transfer for autonomous navigation from the King Abdullah University of Science and Technology, Thuwal, Saudi Arabia, in 2019.

He was with P+Z Engineering as an Electrical Engineer for 3 years, where he worked on the development of mild-hybrid electric machines at BMW. He is currently a Research Scientist with the Intelligent Systems Lab, Intel, Neubiberg, Germany. He has extensive experience in object tracking and autonomous navigation of embodied agents such as cars and unmanned aerial vehicles. His research interests include the fields of computer vision, robotics, and machine learning, where he has contributed to more than ten publications in top tier conference such as Conference on Computer Vision and Pattern Recognition (CVPR), European Conference on Computer Vision (ECCV), International Conference on Computer Vision, Robotics: Science and Systems, International Conference on Robotics and Automation, and International Conference on Intelligent Robots and Systems.

Dr. Müller was recognized as an Outstanding Reviewer for CVPR'18 and won the Best Paper Award at the ECCV'18 workshop UAVision.

Dario Floreano (Senior Member, IEEE) received the M.A. degree in vision psychophysics from Univ. Trieste, Italy, in 1988, the M.S. degree in neural computation from Univ. Stirling, UK, in 1992, and the Ph.D. degree in robotics from Univ. Trieste, Italy, in 1995.

He is a Full Professor and the Director with the Laboratory of Intelligent Systems, Swiss Federal Institute of Technology Lausanne (EPFL), Lausanne, Switzerland. Since 2010, he has also been a Founding Director with the Swiss National Center of Competence in Robotics, Lausanne. He held visiting fellowships with Sony Computer Science Laboratory, Tokyo, Japan; Caltech/JPL, Pasadena, CA, USA; and Harvard University, Boston, MA, USA. His research interests include biologically inspired robotics and artificial intelligence. He has made pioneering contributions to the fields of evolutionary robotics, aerial robotics, and soft robotics. He spun off two robotics companies: senseFly (2009, acquired by the Parrot Group in 2016), which has become a world leader in drones for agriculture and imaging, and Flyability (2015), which is the world leader in inspection drones for confined spaces.

Prof. Floreano served in the Advisory Board of the Future and Emerging Technologies division of the European Commission, has been the Vice-Chair of the World Economic Forum Agenda Council on Smart Systems and Robotics, has been a cofounder of the International Society of Artificial Life, served as an elected member of the Board of Governors of the International Neural Network Society, is on the Advisory Board of the Max-Planck Institute for Intelligent Systems, and has joined the editorial board of ten scientific journals. In 2017, the Economist dedicated a center page portrait to Prof. Floreano (Brain Scan). He also co-organized ten international conferences and several thematic workshops on bioinspired drones and soft robotics, which are now considered foundational events for those communities.